

# Experimentally exploiting quantum hypercorrelations for entanglement-based cryptography

Sebastian Philipp Neumann<sup>1,2\*</sup>, Domenico Ribezzo<sup>1,2</sup>, Martin Bohmann<sup>1,2</sup> and Rupert Ursin<sup>1,2\*</sup>

<sup>1</sup> Institute for Quantum Optics and Quantum Information Vienna, Austrian Academy of Sciences, Boltzmanngasse 3, 1090 Vienna, Austria

<sup>2</sup> Vienna Center for Quantum Science and Technology, Boltzmanngasse 5, 1090 Vienna, Austria

E-mail: [sebastian.neumann@oeaw.ac.at](mailto:sebastian.neumann@oeaw.ac.at), [rupert.ursin@oeaw.ac.at](mailto:rupert.ursin@oeaw.ac.at)

June 2020

**Abstract.** Quantum key distribution (QKD) enables unconditionally secure communication guaranteed by the laws of physics. The last decades have seen tremendous efforts in making this technology commercially feasible, with implementations bridging ever longer distances and creating ever higher secure key rates. Readily deployed glass fiber connections are a natural choice for distributing the single photons necessary for discrete-variable QKD both in intra- and intercity links. Any fiber-based implementation however experiences chromatic dispersion which deteriorates temporal detection precision. This ultimately limits the distance and maximum achievable key rate of any fiber-based QKD system. In this work, we address this limitation to both distance and key rate and present a new method to overcome chromatic dispersion. We exploit the hypercorrelations of entangled photon pairs in wavelength, time and polarization to enable polarization-based QKD free of detrimental dispersion effects. By making use of the inherently quantum-mechanical effect of nonlocal dispersion compensation, we experimentally show an increase in key rate by a factor of 37. Not only can our scheme be used to increase secure key rates, but even to enable QKD in the first place, where insufficient timing precision would lead to excess errors preventing secure communication.

## 1. Introduction

Quantum key distribution (QKD) enables communication partners to exchange messages with unconditional cryptographic security based on the laws of quantum physics rather than assumptions about computational hardness. This decisive advantage of QKD over classical encryption techniques has fostered intensive research since its first proposal in 1984 [1]. The most promising approaches use quantum states of single photons [2]. Glass fibers are an obvious choice for the distribution of such single photon states. This is because existing telecommunication infrastructure can be used, links can be

operated 24/7 independent of weather conditions and time of day, and implementations have low investment thresholds compared to satellite missions [3]. Telecom links are versatile: They can be deployed in network configurations for intra-city links over tens of kilometers [4, 5, 6] but have also been demonstrated in laboratory environments for up to 307 km [7], 404 km [8] and, most recently, 421 km [9] of fiber. In-field QKD using commercially deployed fibers has been shown over a 96 km submarine link [10]. Another QKD demonstration over 66 km of deployed fiber has proven to withstand noise from parallel classical traffic on the same fiber [11].

Now that the principle practicability of long-distance fiber QKD is out of question, the focus of the field is shifting towards issues of optimizing performance [2]. Any commercially viable QKD system's performance will be quantified by its secure key rate, i.e. the number of secure bits acquired by the communication partners (traditionally called Alice and Bob) per second. These bits are read out from measurements on quantum states of single photons. The most crucial performance limit for state-of-the-art QKD implementations is the timing precision used for identifying these single photons at Alice and Bob. This is because successively sent photons and their corresponding bit values must be distinguished from each other in time with high fidelity. If this cannot be guaranteed, the error rate increases, which in turn degrades the key rate or even prohibits distribution of any key at all. Thus, even though quantum sources with high photon generation rates are readily available [12], they have to be operated within the limits set by the whole system's timing precision. So in fact, the most important limit on today's secure key generation rate is the overall timing precision rather than source brightness.

There are three contributions to timing precision: the single photons' coherence time—a fundamental property related to their finite spectral width—, detector timing jitter, and chromatic dispersion of the fibers. Contributions from coherence time and detector jitter can typically be kept in the order of less than ten picoseconds for high-end systems [13, 14] and tens of picoseconds for commercial devices [15, 16]. However, the fiber-specific effect of chromatic dispersion can be substantially larger in connections within metropolitan areas and even more so for long-haul links connecting cities.

This profound limitation to QKD rates has been underrepresented in the scientific discourse up to now. Commercially viable fiber-based QKD will most likely be implemented on conventional, readily deployed optical fibers conforming to the International Telecommunication Union's (ITU) G.652 standard [17], the most popular fiber standard as of now [18]. The widely used Corning SMF-28e+ fiber exhibits a maximum dispersion value of 18 ps/nm/km [19], which we will use for further calculations. Another ITU standard regarding traffic management of different wavelengths on telecom fibers is the dense wavelength division multiplexing (DWDM) grid [20]. It defines wavelength channels for individual signals multiplexed to a single fiber. For a typical 100 GHz channel, the dispersion-induced temporal uncertainty amounts to more than a nanosecond for 100 km links. Thus, chromatic dispersion is by far the most dominant contribution to temporal broadening for long-distance fiber QKD.

However, using state-of-the-art detection equipment, detrimental dispersion effects are visible using less than 10 km of fiber already. It has to be emphasized that this poses a problem for any discrete-variable QKD protocol. This is true independent of the degree of freedom carrying the quantum information that is used to generate the key. Both prepare-and-send and entanglement-based schemes suffer from degradation of timing correlations.

In this work, we implement a method to mitigate the detrimental effect of chromatic dispersion on polarization-based QKD by implementing a nonlocal dispersion compensation scheme [21]. In this way, by exploiting wavelength (anti-)correlation of entangled photons, we can restore tight timing correlations, thus enabling polarization-state measurements with low error rate and increased secure key rate. We realize a full-fledged polarization-based QKD implementation over 6.46 km of fiber and nonlocally compensate for the fiber's dispersion while monitoring the secure key rate. In a realistic scenario of high loss and high noise, we report an increase of the secure key rate by a factor of 37 with the method described.

## 2. Results

### 2.1. Mitigating dispersion effects

The total timing uncertainty of a QKD protocol can be written as

$$\Delta T = \sqrt{\sigma_C^2 + \sigma_J^2 + \sigma_D^2} \quad (1)$$

where  $\sigma_C$  is the photons' coherence time,  $\sigma_J$  is the detector jitter and  $\sigma_D$  is the temporal spread due to chromatic dispersion (in order of increasing importance for modern QKD applications). We assume independent normal distributions for each effect.

For photons of 100 GHz ( $\approx 0.8$  nm) spectral width at 1550 nm, the coherence time  $\sigma_C$  is less than 5 ps. This is negligibly small compared to the influence of detector jitter and chromatic dispersion in current QKD applications using superconducting single-photon nanowire detectors (SSPDs). These devices exhibit the lowest timing jitter values  $\sigma_J$  reported today. They are in the order of 5 ps for telecom wavelengths [13], while commercial devices including time-tagging electronics typically exhibit jitters of 40 ps [15, 22]. The steady advancements in nanowire technology, however impressive they may be, can only be put to use in QKD if chromatic dispersion effects of the links can be mitigated. Without such mitigation, any reduction of  $\sigma_J$  is masked by chromatic dispersion effects, where  $\sigma_D \approx 1400$  ps for a 100 km inter-city link.

But even a comparably short 10 km link in an intra-city network such as in [4, 5] exhibits about 140 ps of dispersion spread, which already poses a problem for high-end QKD implementations. It is therefore of utmost importance for state-of-the-art QKD implementations to overcome dispersion effects.

The chromatic dispersion  $\sigma_D$  in a fiber of length  $L$  is given by

$$\sigma_D = \sigma_\lambda D_\lambda L. \quad (2)$$

Here,  $\lambda$  indicates the central wavelength,  $\sigma_\lambda$  is the spectral width in wavelength of the propagating signal and  $D_\lambda$  ( $[D_\lambda]=\text{ps}/\text{nm}/\text{km}$ ) is the wavelength-dependent dispersion coefficient which is related to the propagation constant  $\beta''$  via  $D_\lambda = -2\pi c\beta''/\lambda^2$  where  $c$  is the speed of light in vacuum [23].

There are several possibilities to keep  $\sigma_D$  low for a fixed fiber length. One is to use photons with a narrow spectrum. Narrow spectra however correspond to longer coherence times  $\sigma_C$ . Even assuming  $\sigma_J=0$ , the optimal trade-off between  $\sigma_D$  and  $\sigma_C$  would still result in  $\Delta T = 113$  ps for a typical 100 km link when optimizing the spectral width.

Another approach is the use of wavelengths in the dispersive medium where  $D_\lambda$  is small. The total dispersion of single-mode glass fibers emanates from both waveguide (i.e., geometric) and material dispersion. Those two effects can be balanced for a certain wavelength such that the total dispersion at this point vanishes, i.e.  $D_\lambda \approx 0$ . The popular G.652 fiber standard requires this zero-crossing of the dispersion slope to be located at  $1312 \pm 12$  nm [17]. Therefore, dispersion effects can be minimized if one deploys photons with wavelengths centered at 1312 nm. However, fiber losses at this wavelength are about 0.3 dB/km as compared to only 0.2 dB/km at 1550 nm (i.e., one order of magnitude more loss over 100 km). Additionally, if implementation in existing telecom infrastructure is desired, the C-band (1530 – 1565 nm) is more commonly used than the O-band (1260 – 1360 nm).

Finally, the most promising method is based on the introduction of equal and oppositely signed dispersion, i.e., dispersion compensation. Experimentally, this can be achieved either by fibers with opposite dispersion or by making use of gratings, e.g., chirped fiber-Bragg gratings [24]. This approach is straightforward for any single-channel application such as the BB84 protocol [1]: One introduces dispersion compensation to the link at some point before the measurement. Thus, if  $D_\lambda^l$  of the link and  $D_\lambda^c$  of the compensation are matched such that  $D_\lambda^l = -D_\lambda^c$ , eq. (2) simply becomes

$$\sigma_D = \sigma_\lambda \underbrace{(D_\lambda^l + D_\lambda^c)}_0 L = 0. \quad (3)$$

For entanglement-based protocols such as BBM92 [25] however, there is a unique method of dispersion compensation developed by Franson [21, 26]. He proposed to carry out so-called nonlocal dispersion compensation for entangled photon pairs by changing the dispersion in one photon channel only. In this way, we can exploit their wavelength correlations to restore temporal correlations which have been degraded due to chromatic dispersion effects. In case of wavelength anti-correlation between entangled photons produced by spontaneous parametric down-conversion (SPDC), the total  $\sigma_D$  between Alice (A) and Bob (B) is equal to the sum of the channels' individual dispersion values:

$$\sigma_D = \sigma_D^A + \sigma_D^B \quad (4)$$

$$= \sigma_\lambda (D_\lambda^A L^A + D_\lambda^B L^B), \quad (5)$$

where  $\sigma_\lambda$  is the photons' effective spectral width in wavelength which is determined by the SPDC source and the filters in use. Therefore,  $\sigma_D = 0$  is possible for zero total

dispersion ( $D_\lambda^A L^A = -D_\lambda^B L^B$ ), reducing  $\Delta T$  to contributions by  $\sigma_C$  and  $\sigma_J$  alone.

It is important to stress that the possibility of nonlocal dispersion compensation is a unique feature of entangled photon-pair sources which makes use of their intrinsic quantum correlations in wavelength to restore their timing correlations. In this sense, it has no classical counterpart and can be considered a quantum advantage. In particular, we exploit quantum correlations in three different degrees of freedom: polarization correlations are used for key generation while wavelength anti-correlations enable compensation of dispersion in time. Thus, the method utilizes quantum hypercorrelations of SPDC photons.

The principal feasibility of nonlocal dispersion compensation has been shown using a broad spectrum centered around the zero-dispersion wavelength of two similar fibers [27]. In this work, we develop the scheme further to demonstrate for the first time that nonlocal dispersion compensation can in fact be used for improving secure key rates in QKD applications. We implemented a full-fledged BBM92 QKD scheme based on polarization-entangled photon pairs sent along standard telecom fibers and show experimentally that by introducing (adjustable) negative dispersion in one channel only, tight timing correlations can be restored and key rates can be increased.

## 2.2. Experimental setup

The working principle of our experimental setup is shown in figure 1. We used a Sagnac-type source of polarization-entangled photons with a type-0 phase-matched nonlinear crystal [28]. It was pumped with a continuous-wave laser at wavelength  $\lambda_p = 775$  nm producing photon pairs with their spectrum centered at approximately 1550 nm via spontaneous parametric down-conversion. The down-converted photons were coupled into a single-mode fiber (SMF). Obeying energy conservation,  $\lambda_p \approx (\lambda_s + \lambda_i)/4$  holds for individual entangled photon-pairs, where s (i) denotes signal (idler) photons. This relation can be used to select entangled signal and idler photons from the full spectrum. To this end, we used dense wavelength division multiplexing (DWDM) top-hat filters with 200 GHz broad spectral transmission [20]. These filters were physically realized by single-mode fibers connected to the exit ports of two successive fiber Bragg gratings transmitting only the desired wavelength range [29]. With two such filters, we realized two 200 GHz wavelength channels centered at 1549.32 and 1550.92 nm, respectively, each carrying one of the entangled photons. We aligned the source such that the photon pairs are created in a hyper-entangled state in the polarization, time, and wavelength degrees of freedom:

$$|\Phi^+\rangle = |\phi^+\rangle_{\text{pol}} \otimes \int d\tau h(\tau) |\tau, \tau\rangle_{\text{time}} \otimes \int d\lambda w(\lambda) |\lambda_0 + \lambda, \lambda_0 - \lambda\rangle_{\text{wl}}. \quad (6)$$

Here,  $h(\tau)$  is a continuous function of time, corresponding to the coherence profile of the laser, and  $w(\lambda)$  characterizes the wavelength distribution around the central wavelength  $\lambda_0$  of the SPDC emission. In the polarization degree of freedom, the photons are prepared in a maximally entangled Bell state

$$|\phi^+\rangle_{\text{pol}} = 1/\sqrt{2}(|H_s, H_i\rangle + |V_s, V_i\rangle)$$

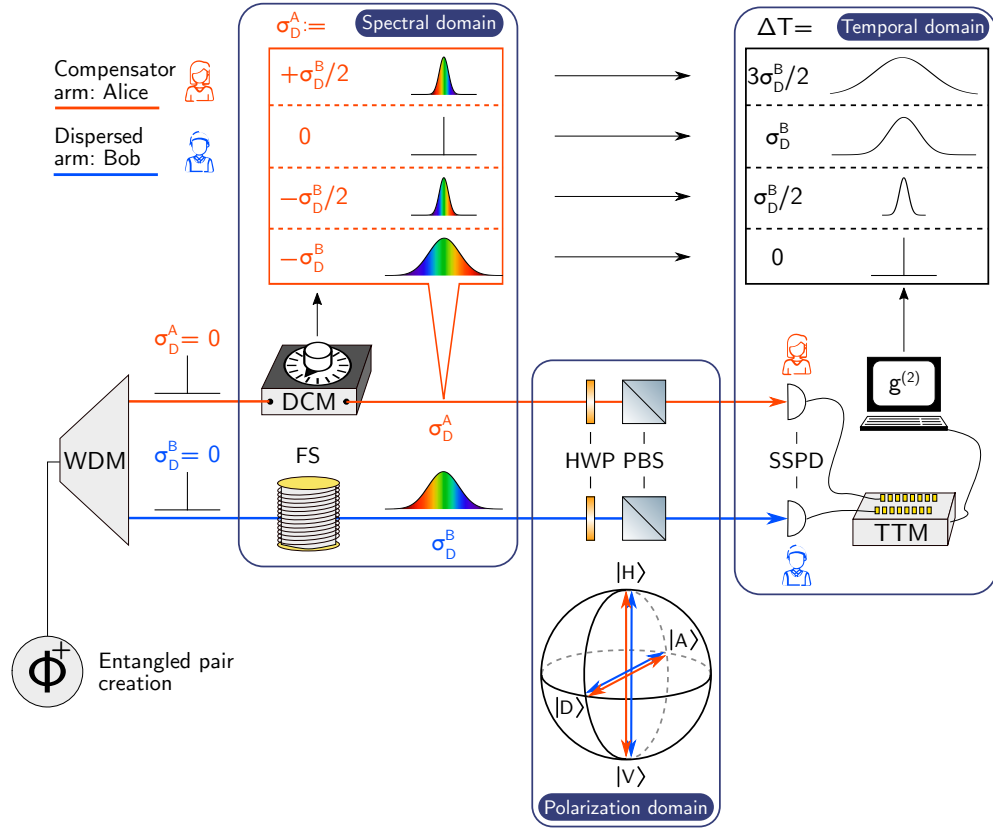


**Figure 1.** Sketch of the experiment's working principle.  $\Phi^+$  denotes the source of photonic entanglement. By making use of wavelength division multiplexing (WDM), two 200 GHz channels guiding the entangled photon pairs are selected from the source spectrum. The photon in the lower arm passes a G.652 telecom fiber spool (FS) where it experiences anomalous (i.e. positively signed) dispersion  $\sigma_D^B$ . The dispersion value in the other arm ( $\sigma_D^A$ ) is manipulated via a dispersion compensation module (DCM). Both photons are measured by Alice and Bob respectively, who record both polarization and arrival time of the photons. This is done by applying different settings of a half-wave plate (HWP) before a polarizing beam splitter (PBS). The transmitted photons are then detected with superconducting single-photon nanowire detectors (SSPD). The detection time is recorded using one time-tagging module (TTM). Using these time tags, we calculate the cross correlation between Alice's and Bob's time stamps to generate the  $g^{(2)}$  intensity-correlation functions displayed in figure 2. Due to the photons' spectral anticorrelation, the resulting temporal width  $\Delta T$  of the correlation function depends on the sum of the individual dispersion values  $|\sigma_D^A + \sigma_D^B|$ . By introducing dispersion of equal magnitude and opposite sign, the initial non-dispersed timing correlations can be restored. In reality, coherence time and detector jitter result in a minimum value for the  $g^{(2)}$  spread, which is not visualized in the sketch for simplicity.

$$= 1/\sqrt{2}(|D_s, D_i\rangle + |A_s, A_i\rangle) \quad (7)$$

where  $H$  ( $V$ ,  $D$ ,  $A$ ) denotes horizontal (vertical, diagonal, antidiagonal) polarization. In what follows, we will exploit the chromatic quantum correlations of the state to restore the tight timing correlations which are scrambled by dispersion. In turn, this regained timing correlations yields an improved secure key rate for the polarization-based cryptography.

We introduced dispersion by injecting the signal photons into a 6.46 km long G.652 telecom fiber with dispersion of  $D_\lambda = 16.7 \pm 1.0$  ps/nm/km specified by the manufacturer [30, 19], resulting in a calculated total dispersion of  $\sigma_D^B/\sigma_\lambda = 107.9 \pm 6.5$  ps/nm. Alice's channel carrying the idler photons was connected to a Teraxion Clearspectrum T2506 dispersion compensation module (DCM). According to the display's reading, it can introduce dispersion values  $\sigma_D^A/\sigma_\lambda$  ranging from  $-170$  to  $+170$  ps/nm in 10 ps/nm steps [31]. Alice and Bob determine the polarization state of their respective photons using polarization analysis modules, consisting of a half-wave plate (HWP) and a polarizing beam splitter (PBS), and detect the photons via superconducting single-photon nanowire detectors (SSPD) of the Single Quantum Eos series connected to a Time Tagger (TTM) Ultra 8 by Swabian Instruments. In order to simulate a long-distance scenario of 300 km distance in terms of loss, we introduced attenuation of about 30 dB in each channel by decreasing the SMF coupling efficiency at the detectors. We estimated the loss using the Klyshko or heralding efficiency, i.e. by determining the ratio between correlated photons and all detector clicks (less noise counts) [32]. Additionally, we report a constant background noise level of 160 kcps (Alice) and 175 kcps (Bob). For every detection event measured by the SSPDs, Alice and Bob recorded a time tag using one time tagger and the HWPs angle setting, corresponding to different polarization measurements ( $0^\circ = H$ ,  $22.5^\circ = D$ ,  $45^\circ = V$ ,  $67.5^\circ = A$ ). The number of coincident events per relative temporal delay between the two detector channels can be plotted as a histogram for each polarization measurement and DCM setting (for  $HH$  see figure 2). Creating such a histogram is equivalent to experimentally obtaining the second-order correlation function  $g^{(2)}$  of the entangled photon pair. The full width at half-maximum (FWHM) of each histogram corresponds to  $\Delta T$ , whose minimum value of approximately 66 ps is given by the detector jitter (coherence time effects are negligible). On top of the jitter, we clearly observe dispersion-induced changes of the histograms' FWHM when tuning the DCM settings over their full range of  $-170$  to  $170$  ps/nm. Figure 3 shows the average FWHMs of all correlations for each of these DCM settings, which we extracted from Gaussian fits to the experimental data. We found each 10 ps/nm step in the DCM settings to induce an average jitter-corrected FWHM change of 7.2 ps. With our method, we were able to tune  $\Delta T$  from 66 to 197 ps by inducing both normal and anomalous dispersion in Alice's arm.

We manipulated the fiber-induced dispersion in a nonlocal manner [26]. This is because the dispersion we introduced in Bob's arm was compensated for by changing solely the dispersion in Alice's arm, while Bob's dispersion value stayed constant. The minimal value of  $\Delta T = 66 \pm 3$  ps was found for a DCM display reading of  $-90$  ps/nm.

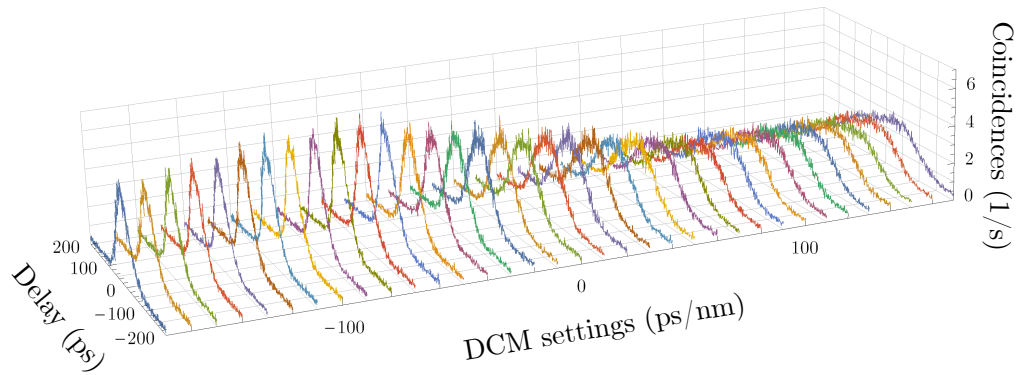


**Figure 2.** Histograms of coincident events according to  $HH$  polarization measurements per relative delay between Alice and Bob in 1 ps bins, normalized to 1 s.  $VV$ ,  $DD$  and  $AA$  (not depicted) show similar behavior. Each histogram corresponds to a different setting of the dispersion compensation module (DCM). Note that DCM settings  $> 0$  ps/nm are equivalent to simulating another dispersive fiber in Alice's arm. The peak values decrease for broader temporal spreads due to constant total coincidence rates.

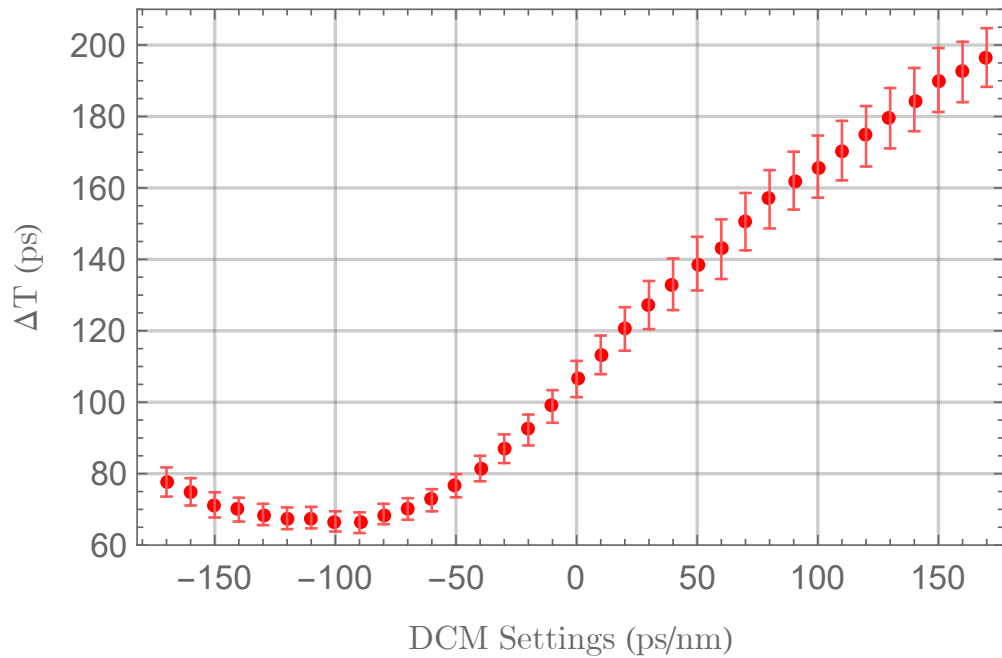


**Figure 3.** Average temporal dispersion  $\Delta T$  as a function of the dispersion compensator module (DCM) settings. The values of  $\Delta T$  were acquired by fitting Gaussian functions to all histograms and averaging over all desired polarization correlations. Errors bars are plotted assuming Poissonian errors of the detection rates. Optimal dispersion compensation was found for the DCM setting of  $-90$  ps/nm, where  $\Delta T$  is limited by the detector jitter  $\sigma_J = 66 \pm 3$  ps. For DCM values of  $-100$  ps/nm and lower, the dispersion in Bob's arm is being overcompensated, thus again increasing the total temporal uncertainty  $\Delta T$ .



The mismatch with the calculated location of the minimal value at  $-108$  ps/nm, which amounts to a 5% deviation in the considered range, can be explained by DCM imperfections and/or deviations of the fiber’s dispersion specification.

### 2.3. Key rate implications

In what follows, we will analyze how exploiting quantum correlations in wavelength and time can enhance the achievable polarization-based QKD rate. Dispersion caused by the optical fiber in a quantum communication realization negatively impacts the secure key rate. To optimize the key rate, one aims to minimize the total temporal uncertainty  $\Delta T$  such that the pair creation rate of the entangled source can be set as high as possible while keeping the influence of noise counts at a minimum. As can clearly be seen in figure 2, the positively signed temporal dispersion  $\sigma_D^B$  introduced by the fiber can be counteracted by introducing negative dispersion coefficients in the DCM. This means that the dispersion-induced degradation of our QKD system’s error rate could be annihilated. Setting the DCM to positive dispersion values however simulates a long-distance fiber link in Alice’s channel, thus further increasing  $\Delta T$ .

To quantify the improvements achieved by our dispersion compensation scheme, we calculated the secure key rate in the asymptotic limit of infinite key size for each DCM setting. In order to do this, one needs to assess several experimental parameters. Firstly, one needs to define which detection events (“clicks”) should be used for creating the secure key. This is achieved by temporal filtering: Those clicks at Alice and Bob which have a certain temporal offset w.r.t. each other, taking into account different travel times and electronical delays, are considered to originate from the same photon pair. The tolerance interval  $t_{CC}$  for this offset is named “coincidence window”. Those counts at Alice and Bob which fall within the window are called “coincidences”. We label coincidences recorded with equal polarization analyzer settings at Alice and Bob as “correct” coincidences, since they are compatible with the state in eq. (7). Coincidences with orthogonal polarization settings are labeled “erroneous”, since they are caused by experimental imperfections not in accordance with eq. (7). The ratio of erroneous coincidences is called quantum bit error rate (QBER,  $E$ ) [2] and can be written as

$$E = \frac{CC_{\text{err}}}{CC_{\text{corr}} + CC_{\text{err}}} \quad (8)$$

where  $CC_{\text{err}}$  ( $CC_{\text{corr}}$ ) is the number of erroneous (correct) coincidences per second. Since the noise level at each detector can be assumed to be uniformly distributed in time, any increase in  $t_{CC}$  causes an increase of the QBER by approximately the same ratio. This is where the harmful effect of dispersion comes in: To account for a dispersion-induced increase in  $\Delta T$ , the coincidence window  $t_{CC}$  also needs to be increased to collect as many desired correlations as possible—at the cost of a higher QBER. Quantitatively, the effect of these parameters on the lower bound for the secure key rate  $R_s$  in the infinite-key limit is given by the formula [33]

$$R_s = CC_{\text{tot}} \cdot (1 - (1 + f)H_2(E)). \quad (9)$$

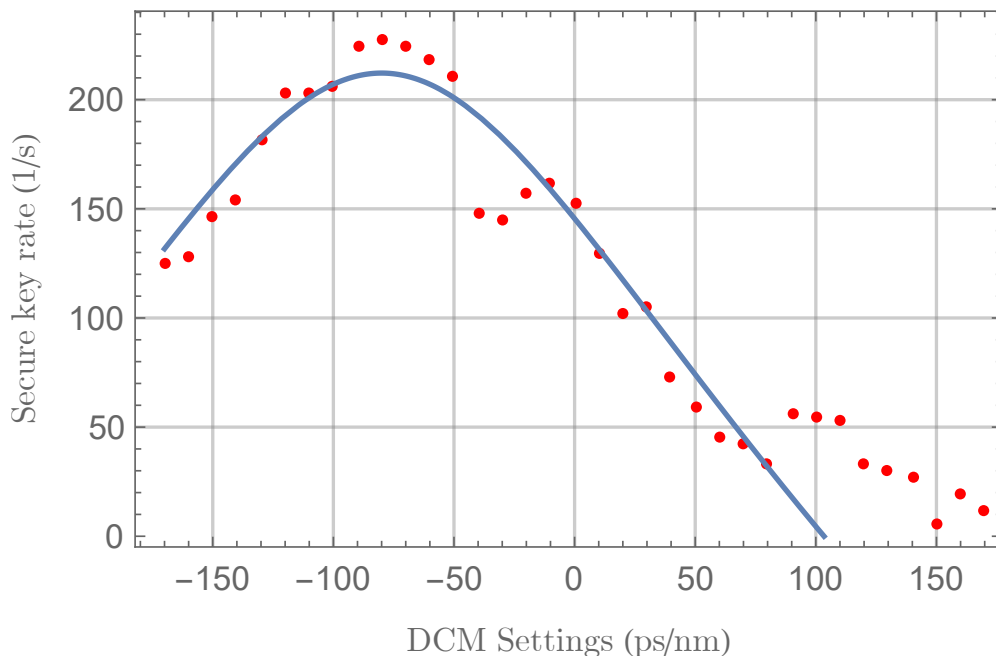


**Figure 4.** Secure key rates for individually optimized coincidence windows  $t_{CC}$  vs. dispersion compensation module (DCM) settings. For a DCM setting of  $-80$  ps/nm, we observed a secure key rate of 228.3 bits/s as compared to just 6.1 bits/s for the least favorable setting. Thus, we observe a 37-fold improvement of the key rate by nonlocal dispersion compensation. The blue graph shows our simple model (see Methods) which captures the main behavior of the experimental data.

Here,  $CC_{\text{tot}} = CC_{\text{corr}} + CC_{\text{err}}$  is the total number of coincidences per second,  $f = 1.1$  [34] is the bi-direction error correction efficiency and  $H_2(x)$  is the binary entropy function.

Using this key rate estimation, we demonstrate the detrimental effect of dispersion and its overcoming by nonlocal dispersion compensation with our measurement data. In particular, we calculated the maximal  $R_s$  for every setting of the DCM module as the average of horizontal-vertical and diagonal-antidiagonal basis settings (see figure 4). We numerically optimized  $t_{CC}$  to acquire the highest secure key rate for each DCM setting individually. The overall maximal secure key rate of 228.3 bits/s is found for the DCM setting at  $-80$  ps/nm. Compared to the lowest acquired value of 6.1 bits/s, our nonlocal dispersion compensation scheme therefore resulted in a 37-fold increase in secure key rate. Furthermore, the observed overall behavior is in good agreement with our theoretical model as can be seen in figure 4. Details on the model are provided in the Methods section.

Thus, we have shown that chromatic dispersion acting on an entangled photon pair can be compensated in a nonlocal manner by manipulating only one of the two entangled photons' dispersion. Doing so, the tight original timing correlations of the entangled source's emission process can be retrieved by exploiting their non-degraded wavelength anticorrelations. To the best of our knowledge, this is the first experimental demonstration of improving secure key rates in QKD via nonlocal

dispersion compensation.

### 3. Discussion

We have devised a QKD implementation over a 6.46 km fiber link and successfully managed to increase the resulting secure key rates by compensating for chromatic dispersion in a nonlocal manner. Utilizing wavelength anticorrelations of polarization-entangled photons to counteract temporal broadening, we have shown a 37-fold gain of key rates compared to the least favorable dispersion configuration. For this nonlocal compensation scheme, a ready-to-use off-the-shelf DCM and patch fibers were deployed, with no need for further alignment of sensitive components. Furthermore, since one device is enough to compensate a two-channel QKD scheme, the DCM insertion loss is the same as it would be in a single-channel experiment. The scheme is therefore ideally suited for real-world applications. Our experiment was designed to match real-life loss and noise scenarios in order to show the feasibility of nonlocal dispersion compensation in entanglement-based QKD. Thus, our findings can easily be generalized to substantially longer fiber links, where control of dispersion is a prerequisite for obtaining high key rates. Taking a typical 300 km link as an example, the secure key rate could be increased by a factor of 400 to about 10 kbit/s with our method. This estimate is ignoring noise counts e.g. from parallel classical traffic, which would increase the necessity of tight timing correlations even further. Concluding, we are convinced that the presented nonlocal dispersion compensation will be an essential component for future implementations of fiber-based QKD networks.

### 4. Methods

The blue curve in figure 4 represents our model of the secure key rate behavior depending on the DCM settings. For this model,  $CC_{\text{tot}}$  in eq. (9) is calculated using the source brightness  $B$ , channel losses  $\eta_i$ , and a correction factor  $s$ :

$$CC_{\text{tot}} = sB\eta_A\eta_B \quad (10)$$

The QBER  $E$  in eq. (8) and eq. (9) is modeled as

$$E \approx \frac{sB\eta_A\eta_B e_o + \xi/2}{sB\eta_A\eta_B + \xi} \quad (11)$$

where  $e_o$  is the probability of erroneous detection due to optical imperfections of source and polarization analyzers,  $DC_i$  are the noise counts per detector and

$$\xi = (B\eta_A + 2DC_A)(B\eta_B + 2DC_B)\sqrt{\sigma_T^2 + \sigma_D^2} \quad (12)$$

is the rate of coincident counts which arise by chance due to the finite coincidence window  $t_{\text{CC}}$  and not due to an actual photon pair.  $\xi$  is divided by 2 in the numerator of eq. (11) because only half of these “accidental” clicks contribute to erroneous coincidences with orthogonal polarizer settings and the other half is registered as correct. For simplicity, we do not account for the numerical optimization of the coincidence window in our

model, but set  $t_{CC} = \Delta T$ . The factor  $s = \text{erf}[\sqrt{\ln(2)}] = 0.76$  in eq. (10) and eq. (11) therefore accounts for the fact that true coincidence clicks originating from photon pairs follow a Gaussian distribution with FWHM  $\Delta T$ , i.e. clicks outside the coincidence window at the “tails” of the distribution are lost.

Figure 4 shows this key rate model for the following parameters in use:  $B = 5.75 \times 10^8$  cps,  $\eta_1 = 29.05$  dB,  $\eta_2 = 29.31$  dB,  $DC_1 = 1.4 \times 10^5$  cps,  $DC_2 = 1.75 \times 10^5$  cps,  $e_o = 0.01$ ,  $\sigma_J = 66$  ps. All modeling parameters were estimated from experimental data. The model was offset by  $-80$  ps in order to fit the data, although we expected optimal compensation to take place for  $-90$  ps. This discrepancy is most likely due to statistical fluctuations in the measured count rates and will be subject of future studies. Further deviations between our model and the observed  $R_s$  can be explained by the fact that our simple model does not capture the numerically obtained optimal coincidence windows, which is especially important for low key rates, and that all underlying distributions were assumed to be perfectly Gaussian for simplicity. Nevertheless, we observe that our model correctly captures the main features of the experimentally obtained key rates and thus explains the functional dependence of the secure key rate on the nonlocal dispersion compensation.

## References

- [1] C. H. Bennett and G. Brassard. Quantum cryptography: public key distribution and coin tossing int. In *Conf. on Computers, Systems and Signal Processing (Bangalore, India, Dec. 1984)*, pages 175–9, 1984.
- [2] F. Xu, X. Ma, Q. Zhang, H.-K. Lo, and J.-W. Pan. Secure quantum key distribution with realistic devices. *Rev. Mod. Phys.*, 92:025002, May 2020.
- [3] J. Yin, Y.-H. Li, S.-K. Liao, M. Yang, Y. Cao, L. Zhang, J.-G. Ren, W.-Q. Cai, W.-Y. Liu, S.-L. Li, R. Shu, Y.-M. Huang, L. Deng, L. Li, Q. Zhang, N.-L. Liu, Y.-A. Chen, C.-Y. Lu, X.-B. Wang, F. Xu, J.-Y. Wang, C.-Z. Peng, A. K. Ekert, and J.-W. Pan. Entanglement-based secure quantum cryptography over 1,120 kilometres. *Nature*, 582(7813):501–505, Jun 2020.
- [4] S. K. Joshi, D. Aktas, S. Wengerowsky, M. Lonari, S. P. Neumann, B. Liu, T. Scheidl, Z. Samec, L. Kling, A. Qiu, M. Stipevi, J. G. Rarity, and R. Ursin. A trusted-node-free eight-user metropolitan quantum communication network. *Preprint at <https://arxiv.org/abs/1907.08229>*, 2019.
- [5] J. F. Dynes, A. Wonfor, W. W.-S. Tam, A. W. Sharpe, R. Takahashi, M. Lucamarini, A. Plevs, Z. L. Yuan, A. R. Dixon, J. Cho, Y. Tanizawa, J.-P. Elbers, H. Grei er, I. H. White, R. V. Penty, and A. J. Shields. Cambridge quantum network. *npj Quantum Information*, 5(1):101, Nov 2019.
- [6] D. Bacco, I. Vagniluca, B. Da Lio, N. Biagi, A. Della Frera, D. Calonico, C. Toninelli, F. S. Cataliotti, M. Bellini, L. K. Oxenl we, et al. Field trial of a three-state quantum key distribution scheme in the florence metropolitan area. *EPJ Quantum Technology*, 6(1):5, 2019.
- [7] B. Korzh, C. C. W. Lim, R. Houlmann, N. Gisin, M. J. Li, D. Nolan, B. Sanguinetti, R. Thew, and H. Zbinden. Provably secure and practical quantum key distribution over 307 km of optical fibre. *Nature Photonics*, 9(3):163–168, Mar 2015.
- [8] H.-L. Yin, T.-Y. Chen, Z.W. Yu, H. Liu, L.-X. You, Y.-H. Zhou, S.-J. Chen, Y. Mao, M.-Q. Huang, W.-J. Zhang, H. Chen, M. J. Li, D. Nolan, F. Zhou, X. Jiang, Z. Wang, Q. Zhang, X.-B. Wang, and J.-W. Pan. Measurement-device-independent quantum key distribution over a 404 km optical fiber. *Physical Review Letters*, 117(19):190501, 2016.

- [9] A. Boaron, G. Boso, D. Rusca, C. Vulliez, C. Autebert, M. Caloz, M. Perrenoud, G. D. M. Gras, F. Bussieres, M.-J. Li, D. Nolan, A. Martin, and H. Zbinden. Secure quantum key distribution over 421 km of optical fiber. *Physical Review Letters*, 121(190502), 2018.
- [10] S. Wengerowsky, S. K. Joshi, F. Steinlechner, J. R. Zichi, S. M. Dobrovolskiy, R. van der Molen, J. W. N. Los, V. Zwiller, M. A. M. Versteegh, A. Mura, D. Calonico, M. Inguscio, H. Hübel, L. Bo, T. Scheidl, A. Zeilinger, A. Xuereb, and R. Ursin. Entanglement distribution over a 96-km-long submarine optical fiber. *Proceedings of the National Academy of Sciences*, 116(14):6684–6688, 2019.
- [11] Y. Mao, B.-X. Wang, C. Zhao, G. Wang, R. Wang, H. Wang, F. Zhou, J. Nie, Q. Chen, Y. Zhao, et al. Integrating quantum key distribution with classical communications in backbone fiber network. *Optics express*, 26(5):6010–6020, 2018.
- [12] F. Steinlechner, S. Ramelow, M. Jofre, M. Gilaberte, T. Jennewein, J. P. Torres, M. W. Mitchell, and V. Pruneri. Phase-stable source of polarization-entangled photons in a linear double-pass configuration. *Opt. Express*, 21(10):11943–11951, May 2013.
- [13] B. Korzh, Q.-Y. Zhao, J. P. Allmaras, S. Frasca, T. M. Autry, E. A. Bersin, A. D. Beyer, R. M. Briggs, B. Bumble, M. Colangelo, G. M. Crouch, A. E. Dane, T. Gerrits, A. E. Lita, F. Marsili, G. Moody, C. Peña, E. Ramirez, J. D. Rezac, N. Sinclair, M. J. Stevens, A. E. Velasco, V. B. Verma, E. E. Wollman, S. Xie, D. Zhu, P. D. Hale, M. Spiropulu, K. L. Silverman, R. P. Mirin, S. W. Nam, A. G. Kozorezov, M. D. Shaw, and K. K. Berggren. Demonstration of sub-3 ps temporal resolution with a superconducting nanowire single-photon detector. *Nature Photonics*, 14(4):250–255, Apr 2020.
- [14] I. E. Zadeh, J. W. N. Los, R. B. M. Gourgues, J. Chang, A. W. Elshaari, J. Zichi, Y. J. van Staaden, J. Swens, N. Kalhor, A. Guardiani, Y. Meng, K. Zou, S. Dobrovolskiy, A. W. Foghini, D. R. Schaart, D. Dalacu, P. J. Poole, M. E. Reimer, X. Hu, S. F. Pereira, V. Zwiller, and S. N. Dorenbos. A platform for high performance photon correlation measurements. *Preprint at <https://arxiv.org/abs/2003.09916>*, 2020.
- [15] Single Quantum, <https://singlequantum.com/wp-content/uploads/2019/05/Single-Quantum-Eos.pdf>. *Single Quantum Eos SNSPD Closed-Cycle System Data Sheet*, 2020.
- [16] ID QUantique, [https://marketing.idquantique.com/acton/attachment/11868/f-023b/1/-/-/-/ID281\\_Brochure.pdf](https://marketing.idquantique.com/acton/attachment/11868/f-023b/1/-/-/-/ID281_Brochure.pdf). *ID Quantique ID281 Superconducting nanowire system Data Sheet*, 2020.
- [17] Recommendation G.652 (11/16), May 2017.
- [18] S. Warier. *Engineering optical networks*. Artech House, Norwood, MA :, 2018.
- [19] Single Quantum, <https://singlequantum.com/wp-content/uploads/2019/05/Single-Quantum-Eos.pdf>. *Corning SMF 28 Ultra Optical Fiber Product Information*, 2020.
- [20] Recommendation G.694.1 (12/2003), February 2012.
- [21] J. D. Franson. Nonlocal cancellation of dispersion. *Physical Review A*, 45(5):3126, 1992.
- [22] Swabian Instruments, <https://www.swabianinstruments.com/static/downloads/TimeTagger.pdf>. *Swabian Instruments Time Tagger Series*, 2020.
- [23] M. C. Teich B. E. A. Saleh. *Fundamentals of Photonics*. Wiley, 2nd edition, February 2007.
- [24] S. Ramachandran. *Fiber Based Dispersion Compensation*. Optical and Fiber Communications Reports. Springer New York, 2007.
- [25] C. H. Bennett, G. Brassard, and N. D. Mermin. Quantum cryptography without bells theorem. *Physical Review Letters*, 68(5):557, 1992.
- [26] J. D. Franson. Nonclassical nature of dispersion cancellation and nonlocal interferometry. *Physical Review A*, 80(3):032119, 2009.
- [27] J. A. Grieve, Y. Shi, H. S. Poh, C. Kurtsiefer, and A. Ling. Characterizing nonlocal dispersion compensation in deployed telecommunications fiber. *Applied Physics Letters*, 114(13):131106, 2019.
- [28] O. Gayer, Z. Sacks, E. Galun, and A. Arie. Temperature and wavelength dependent refractive index equations for mgo-doped congruent and stoichiometric linbo3. *Applied Physics B*, 91(2):343–348, May 2008.

- [29] K. Grobe. *Wavelength division multiplexing: A practical engineering guide*. Wiley series in pure and applied optics. Wiley, Hoboken, New Jersey, first edition edition, 2008.
- [30] Personal communication with Dr.-Ing. Frank Depiereux, fionec GmbH.
- [31] Unfortunately, we cannot give more detailed information about the device, since production is discontinued by the manufacturer and neither data sheet nor manual are available to us.
- [32] D. N. Klyshko. Use of two-photon light for absolute calibration of photoelectric detectors. *Soviet Journal of Quantum Electronics*, 10(9):1112–1117, sep 1980.
- [33] X. Ma, C.-H. F. Fung, and H.-K. Lo. Quantum key distribution with entangled photon sources. *Physical Review A*, 76(1):012307, 2007.
- [34] D. Elkouss, A. Leverrier, R. Alléaume, and J. J. Boutros. Efficient reconciliation protocol for discrete-variable quantum key distribution. In *Information Theory, 2009. ISIT 2009. IEEE International Symposium on*, pages 1879–1883. IEEE, 2009.

## Acknowledgments

We acknowledge European Unions Horizon 2020 programme grant agreement No. 857156 (OpenQKD) and the Austrian Academy of Sciences. We also want to thank Josef Vojtech of CESNET (Prague) for providing us with dispersion compensation equipment, Siddarth Koduru Joshi of NSQI (Bristol) for lending us a DWDM device and Sren Wengerowsky of IQOQI (Vienna) for fruitful discussions.

## 5. Author Contributions

S.N. and R.U. devised the experiment. S.N. and D.R. built the measurement setup. D.R. collected measurement data. S.N., D.R. and M.B. analyzed the data. R.U. supervised the work. S.N., M.B. and R.U. contributed to write the paper.

## 6. Competing Interests

The authors declare no competing interests.

## 7. Additional Information

**Correspondence** and requests for materials should be addressed to S.N. and R.U.